ELSEVIER

Biochimica et Biophysica Acta 1460 (2000) 133–156

BIOCHIMICA ET BIOPHYSICA ACTA
BBA

www.elsevier.com/locate/bba

Review

Atomic resolution structures of bacteriorhodopsin photocycle intermediates: the role of discrete water molecules in the function of this light-driven ion pump

Hartmut Luecke

Departments of Molecular Biology and Biochemistry and Physiology and Biophysics, UCI Program in Macromolecular Structure, University of California, Irvine, CA 92697-3900, USA

Received 24 March 2000; accepted 24 March 2000

Abstract

High-resolution X-ray crystallographic studies of bacteriorhodopsin have tremendously advanced our understanding of this light-driven ion pump during the last 2 years, and emphasized the crucial role of discrete internal water molecules in the pump cycle. In the extracellular region an extensive three-dimensional hydrogen-bonded network of protein residues and seven water molecules leads from the buried retinal Schiff base via water 402 and the initial proton acceptor Asp85 to the membrane surface. Near Lys216 where the retinal binds, transmembrane helix G contains a π-bulge that causes a non-proline kink. The bulge is stabilized by hydrogen bonding of the main chain carbonyl groups of Ala215 and Lys216 with two buried water molecules located in the otherwise very hydrophobic region between the Schiff base and the proton donor Asp96 in the cytoplasmic region. The M intermediate trapped in the D96N mutant corresponds to a late M state in the transport cycle, after protonation of Asp85 and release of a proton to the extracellular membrane surface, but before reprotonation of the deprotonated retinal Schiff base. The M intermediate from the E204Q mutant corresponds to an earlier M, as in this mutant the Schiff base deprotonates without proton release. The structures of these two M states reveal progressive displacements of the retinal, main chain and side chains induced by photoisomerization of the retinal to 13-*cis*,15-*anti*, and an extensive rearrangement of the three-dimensional network of hydrogen-bonded residues and bound water that accounts for the changed pK_as of the Schiff base, Asp85, the proton release group and Asp96. The structure for the M state from E204Q suggests, moreover, that relaxation of the steric conflicts of the distorted 13-*cis*,15-*anti* retinal plays a critical role in the reprotonation of the Schiff base by Asp96. Two additional waters now connect Asp96 to the carbonyl of residue 216, in what appears to be the beginning of a hydrogen-bonded chain that would later extend to the retinal Schiff base. Based on the ground state and M intermediate structures, models of the molecular events in the early part of the photocycle are presented, including a novel model which proposes that bacteriorhodopsin pumps hydroxide (OH^-) ions from the extracellular to the cytoplasmic side.

Keywords: High-resolution membrane protein structure; Light-driven ion transport; Ion pump mechanism

1. Introduction

Bacteriorhodopsin (BR) is a highly efficient light-driven ion pump in *Halobacterium salinarum* where

E-mail: hudel@uci.edu

0005-2728/00/$ – see front matter
PII: S0005-2728(00)00135-3

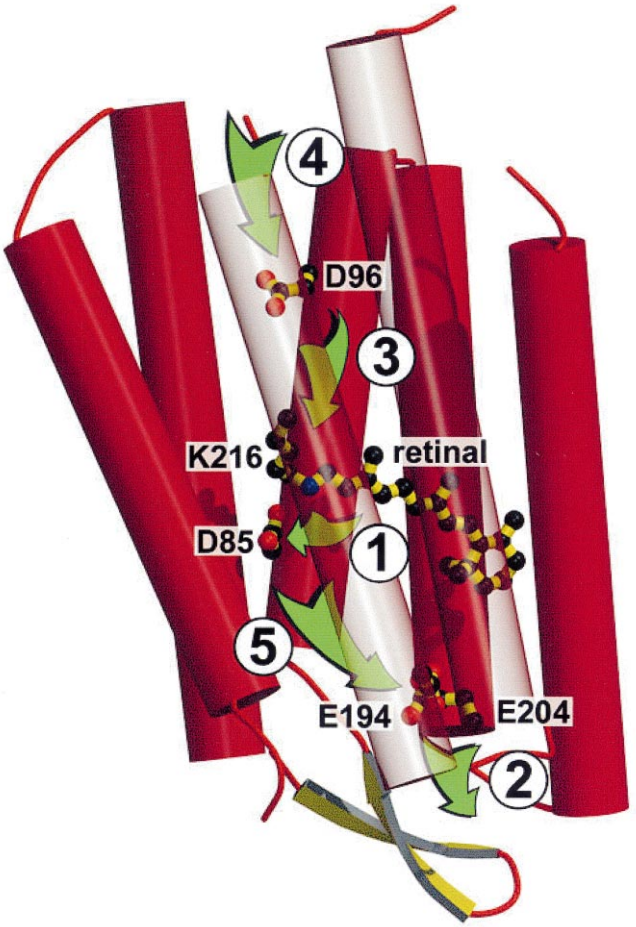

Fig. 1. Overall view of bacteriorhodopsin, shown with the retinal and residues directly implicated in ion transport. Standard orientation with cytoplasmic side on top. The arrows indicate proton transfer steps during the wild-type photocycle. The numbers refer to their sequential order after the initial photon-driven isomerization of the retinal: (1) deprotonation of the Schiff base, protonation of Asp85, yielding the early M intermediate; (2) proton release from the proton release group to the extracellular surface, yielding the late M intermediate; (3) deprotonation of Asp96, reprotonation of the Schiff base, yielding the N intermediate; (4) reprotonation of Asp96 from the cytoplasmic surface, thermal reisomerization of the retinal, yielding the O intermediate; (5) deprotonation of Asp85, reprotonation of the proton release group, regenerating the ground state.

it generates an electrochemical ion gradient that is subsequently converted into chemical energy by a second integral membrane protein, ATP synthase. Bacteriorhodopsin has been the subject of nearly three decades of intense investigation, yielding a wealth of biochemical, spectroscopic, mutational and structural information (recently reviewed in [1–4]), making it the best understood ion pump. BR is a homologue of the light-driven chloride pump halorhodopsin [5,6], sensory rhodopsins [7], and the structural prototype of the large family of G protein-coupled receptors and other proteins that contain multiple transmembrane helices. It is a small 26 kDa protein of seven transmembrane helices with short interhelical loops and extramembrane N- and C-termini.

Throughout the literature, BR is described as a light-driven pump that transports protons (H^+) against an electrochemical gradient from the cytoplasmic to the extracellular side. This process is energized by photoisomerization of the covalently attached all-*trans* retinal chromophore to the 13-*cis*, 15-*anti* configuration. A general scheme of the key events in the transport cycle that follows is shown in

Fig. 1. Understanding how these processes cause the unidirectional translocation of ions requires detailed knowledge of the structural changes in the K, L, M, N and O intermediates. However, the crucial intermediate is the M state, because in M the Schiff base is deprotonated, Asp85 to its extracellular side is protonated, and a proton has been released to the surface, but Asp96 to its cytoplasmic side has not yet become deprotonated (after step 2 but before step 3 in Fig. 1).

This review focuses on the recently determined atomic resolution structures of BR in the ground ('BR') state and structures of photocycle intermediates. The implications of these structures and structural changes for the pumping mechanism and its vectoriality will be discussed. Several models of the molecular steps in the early part of the photocycle will be presented, including a novel mechanism that proposes net hydroxide transport at the retinal Schiff base, in the direction opposite to the commonly presented proton transport scheme.

1.1. Ion pumps

Active transport of ions against their electrochemical gradient across cell and organelle membranes is carried out by proteins that couple an energy-yielding reaction, such as hydrolysis of ATP, electron transfer, or the isomerization of retinal, to the transmembrane movement of ions [8]. To date, a major unsolved problem of membrane bioenergetics is the molecular mechanism of this type of transport. Mechanisms with predictive ability must be able to explain in atomic detail how the free energy from the driving reaction is utilized to change, in an ordered way, the conformations and affinities of binding sites for the transported ion. Crystallographic structures are available only for a few transport proteins, and a major effort is currently expended to improve their resolutions to derive detailed mechanisms of the pumping processes. One milestone in any X-ray structure determination is the point at which the positions of ordered water molecules become evident as positive density features in F_o-F_c and $2F_o-F_c$ maps. Although essential to fully understand ion pumping, for integral membrane proteins this level of detail has been achieved in only a few cases.

1.2. The photocycle by spectroscopic and mutational studies

A large portion of the information now available about the bacteriorhodopsin photocycle has been derived and accumulated by increasingly sophisticated spectroscopic and mutational studies [1–4]. The protonation state of the Schiff base and various carboxylates has been studied by time-resolved visible [9] and infrared spectroscopy [10]. Nuclear magnetic resonance (NMR) [11] and resonance Raman spectroscopy [12] have yielded detailed information about the conformation of the retinal.

Fig. 1 depicts the key events during the photocycle and the following list summarizes the salient features of each of the photocycle intermediates BR, K, L, M, N and O:

- **The ground (or 'BR') state** ($\lambda_{max} = 568$ nm) is the best-defined state, both in terms of ionization states and structure. The light-adapted form contains an active site with the all-*trans* retinal in tight contact with surrounding protein residues, and the protonated Schiff base in direct hydrogen-bonding contact to water 402 [13,14]. Towards the extracellular side, an extensive hydrogen-bonded network leads from the Schiff base via water 402, deprotonated Asp85, W406, Arg82 and additional waters to the initially protonated terminal proton release group (Glu204/Glu194) near the extracellular surface. This network is presumably the cause for the observed proton equilibration between the Schiff base and the bulk ($T_{1/2} \sim 0.5$ ms [15]). In marked contrast, the cytoplasmic side is very hydrophobic, with no polar residues or ordered waters between the Schiff base and protonated Asp96.
- **The K state** ($\lambda_{max} = 590$ nm) arises within a few picoseconds of photon absorption, depositing about 50 kcal/mol of energy into the retinal. The K state has a reported ΔH of 11.6 kcal/mol, thus about 20% of the photon energy is converted to enthalpy and a substantial portion of this enthalpy gain is due to charge separation [16,17]. Spectroscopic methods have determined a highly strained (twisted) 13-*cis*,15-*anti* configuration of the retinal in this state as evidenced by large-amplitude hydrogen-out-of-plane vibrations [18–20].

- **In the L state** (λ_{max} = 550 nm), the retinal strain has partly relaxed and hydrogen bonds of the retinal, protein groups and bound waters begin to change [21]. The conformation at this point in the photocycle is of particular importance as the active site is now primed for the decisive event in the photocycle, the protonation of Asp85 and the deprotonation of the Schiff base (L to M reaction).
- **The M state** (λ_{max} = 412 nm) is defined by a deprotonated Schiff base and consists of at least two substates, often referred to as M_1 and M_2 [22]. For this reaction to proceed, the large initial pK_a difference of over 11 units between the proton donor (Schiff base, ground state pK_a of over 13) and the proton acceptor (Asp85, ground state pK_a of 2) has to be reduced to less than one unit. Kinetic studies on purple membrane suspensions have suggested that in these substates the retinal Schiff base comes to two sequential protonation equilibria with the proton acceptor toward the extracellular side, Asp85, equilibria that are shifted further to deprotonation of the Schiff base in M_2 [23]. At this point, reprotonation of the Schiff base from Asp85 is no longer possible.
- **In the N state** (λ_{max} = 560 nm) the Schiff base has been reprotonated while Asp96 to the cytoplasmic side has deprotonated [24]. With Asp85 still protonated and Asp96 now deprotonated, the retinal binding site is relaxed and accommodates preferentially the 13-*cis*,15-*anti* configuration [25].
- **The O state** (λ_{max} = 610 nm) occurs after both reprotonation of Asp96 from the cytoplasmic side and thermal reisomerization of the retinal. The driving force for its transition to BR is not clear, but it is the last and unidirectional step of the photocycle in which the initially very low pK_a of Asp85 is reestablished, and this residue deprotonates in a strongly downhill reaction to reprotonate the extracellular proton release site [26,27], or when a proton was not released from this site in the L to M reaction, presumably to release a proton directly to the surface.

1.3. Structural methods

In addition to spectroscopic investigations, a large amount of structural information about BR and its photocycle intermediates has been obtained, with steadily increasing resolution and accuracy. Notable methods employed were electron microscopy of two-dimensional crystals in projection [28], later expanded to three-dimensional electron diffraction ([29–31], Subramaniam and Henderson, this volume). Valuable information also came from X-ray diffraction on two-dimensional crystals [32], and more recently from site-directed spin labeling in electron paramagnetic resonance studies which yields time-resolved distance and environment changes of specific residues [33], and atomic force microscopy [34].

2. Overall comparison of published atomic structures

Currently, the Protein Data Bank [35] contains 20 atomic coordinate entries of bacteriorhodopsin structures. This large number attests to the fact that bacteriorhodopsin is one of the most-studied and best-understood integral membrane proteins. Of these 20 coordinate entries, two are theoretical models (1BAC, 1BAD) and three are NMR structures of fragments (1BCT, 1BHA, 1BHB) which will not be discussed further in this review. Of the remaining 15 entries, four are electron diffraction structures (1BRD, 2BRD, 1AT9, 2AT9), with the former two representing the pioneering work by Henderson and coworkers that produced the first atomic level models of bacteriorhodopsin [30]. The remaining 11 entries are X-ray crystallographic structures to varying resolutions. Seven of these describe the ground (or light-adapted) state (1AP9, 1BM1, 1BRR, 1BRX, 1C3W, 1C8R, 1QHJ), while four describe the structures of cryo-trapped photocycle intermediates (1C8S, 1QKO, 1QKP, 1CWQ). One of these (1CWQ) has been released without an accompanying publication and will not be discussed here.

Table 1 shows the result of a least-squares alignment of the structures currently deposited at the Protein Data Bank with the highest-resolution structure (1C3W, 1.55 Å) [14]. The root-mean-square (RMS) deviation between aligned structures is listed for main chain atoms, side chain atoms and all atoms. The four electron diffraction studies show improved accuracy with increasing level of refinement and resolution. 1BRD [30] and 2BRD [31] can be regarded as the grandparents of today's high-resolution struc-

Table 1
Overall comparison of deposited atomic bacteriorhodopsin structures with the highest resolution structure (1C3W, 1.55 Å resolution [14]

PDB code	Main chain RMS (Å)	Side chain RMS (Å)	All atom RMS (Å)	Resolution (Å)	Method
1BRD	2.05	–	–	3.5	ED
2BRD	1.88	3.55	2.82	3.5	ED
1AT9	1.19	2.00	1.63	3.0	ED
2AT9	1.28	1.68	1.49	3.0	ED
1AP9[a]	2.11	3.46	–	2.35	X-ray, CLP
1AP9	1.68	3.28	2.58	2.35	X-ray, CLP
1QHJ[b]	0.46	1.14	0.86	1.9	X-ray, CLP
1QKO[c]	0.48	1.18	0.89	2.1	X-ray, CLP
1QKP[c]	0.48	1.17	0.89	2.1	X-ray, CLP
1CWQ[d]	1.21	2.01	1.64	2.3	X-ray, CLP
1CWQ[e]	1.34	2.19	1.81	2.3	X-ray, CLP
1BM1	0.89	2.15	1.63	3.5	X-ray, detergent
1BRR[f]	1.04	1.67	1.40	2.9	X-ray, detergent
1BRX[g]	0.41	1.12	0.83	2.3	X-ray, CLP
1C8R	0.19	0.30	0.25	1.8	X-ray, CLP
1C8S[h]	0.55	0.98	0.79	2.0	X-ray, CLP

The main chain atoms of the deposited bacteriorhodopsin structures were aligned with 1C3W, using the program Swiss-PdbViewer [94]. The RMS deviation between the aligned structures is given for main chain atoms only, side chain atoms only, and for all atoms.
[a]1AP9 as published in [40] and pre-released in January 1998.
[b]When discarding residues 5 and 6. With residues 5 and 6 included, the alignment values increase to 0.88 Å, 1.28 Å and 1.09 Å, respectively.
[c]Low-temperature K intermediates of wild type, based on entry 1QHJ.
[d]Molecule A (ground state) of deposited file without publication.
[e]Molecule B (M state) of deposited file without publication.
[f]Best of the three molecules in the asymmetric unit.
[g]An accusation by Ceska that the 1BRX coordinates were changed between the time of publication and PDB deposition [95] has been retracted recently in an Erratum [96].
[h]M intermediate of D96N mutant.

tures. However, it should be noted that despite the fact that 2BRD served as the starting model for subsequent atomic-resolution structure determinations, the higher resolution structures, in particular the ones at resolutions better than 2 Å, clearly have sufficiently high observations-to-parameters ratios to overcome the problem of model bias. In particular, the 1.55 Å ground state structure is based on 32 249 unique, experimentally observed reflection intensities for 1975 atoms (or 8300 refinable parameters and an observations-to-parameters ratio of 3.9), further augmented by 8209 stereochemical restraints employed during refinement [14].

Contrary to a recent review article [36] which insinuated that the refinement of the structure from these crystals had been carried out by the questionable means of de-twinning the original strongly twinned reflection intensities, refinement of the merohedrally twinned X-ray diffraction data was not carried out by de-twinning, but rather by refining against the unmodified experimental reflection intensities, taking the contribution of both twins into account while refining their relative fractions on every cycle [37].

The majority of high-resolution bacteriorhodopsin structures are based on crystals grown by the recently developed cubic lipid phase (CLP) crystallization method ([38,39], Landau et al., this volume). However, two of the three structures by the groups of Rosenbusch and Pebay-Peyroula were compromised by their failure to realize the presence of strong merohedral twinning (1AP9[a] in Table 1) [40] and later by only partially correcting merohedral twinning for the final PDB entry 1AP9.

Table 2
Buried surface area [67] of various bacteriorhodopsin oligomers in the 1.55 Å structure

Bacteriorhodopsin oligomer	Buried surface area (%)
Monomer	0
Trimer	13.9
Purple membrane without lipids	15.1
Lipid–trimer contacts	39.6
Purple membrane with lipids	54.7

Forming a trimer from three monomers buries about 14% of the accessible surface. Trimer–trimer contacts in the bilayer (*a*/*b*) plane contribute very little (1.2%), whereas protein–lipid contacts bury an additional 40% of the surface area.

One notable exception to the CLP-based structures is the structure 1BRR [41] which was determined from crystals grown by the traditional detergent-assisted vapor diffusion method [42,43]. Despite the lower nominal resolution of this structure (2.9 Å), the fact that it contained three independent copies of the bacteriorhodopsin monomer per asymmetric unit and the correspondingly high number of observations per parameter resulted in a well-defined protein structure in good agreement with the current high-resolution structures.

2.1. The overall structure

As is evident from the alignment in Table 1, the peptide backbone of this seven-transmembrane helical protein is very similar to that described in the initial reports at 3.5 Å resolution [30,31]. The largest differences from earlier models are in the loop regions, helix G, and in the side chains (Table 2). The B–C interhelical loop forms a twisted anti-parallel β-sheet on the extracellular surface, stabilized by six hydrogen bonds. Bacteriorhodopsin monomers form a very tight trimeric unit that is stabilized by extensive hydrophobic helix–helix contacts which bury 1376 $Å^2$ (13.9% of each monomer surface), but also includes intermolecular salt bridges between Lys40 and Asp104 [14,41].

In addition to providing more accurate positions of the protein and chromophore atoms, high-resolution diffraction studies (to 2.3 Å and better) also are capable of locating ordered water molecules, long thought to play a central role in the photocycle of bacteriorhodopsin (reviews in this issue by Kandori et al. and Dencher et al.). The positions of the first ordered internal waters were reported in the 2.3 Å structure by Luecke et al. [13], including water 402 which is hydrogen-bonded at a crucial position between the ion pair of the protonated Schiff base and Aps85.

The 1.55 Å ground state structure now available unambiguously identifies the configuration of the retinal and its binding site, specifies all residue and backbone interactions, locates all hydrogen-bonded water molecules in the protein interior, and describes the arrangement of lipids in the surrounding bilayer [14]. A recently published 1.9 Å resolution study by Pebay-Peyroula and coworkers [44] using non-twinned CLP crystals is now in excellent agreement with the 1.55 Å structure with the exception of water 502 in the cytoplasmic region. The structural details of the high-resolution ground state and intermediate structures and their implications for ion pumping will be discussed in the following sections.

3. Details of high-resolution atomic structures

3.1. The ground state

The ground or 'BR' state commonly refers to the all-*trans* configuration of the retinal chromophore as generated by illumination with white light (called light adaptation). The following sections are based on the 1.55 Å structure determined from partially merohedrally twinned crystals (1C3W) [14], but with few exceptions are supported by the 1.9 Å structure of the same crystal form determined in the absence of twinning [44].

3.1.1. The region of the retinal

The configuration of the all-*trans* retinal and surrounding protein and water moieties is clearly defined in the electron density maps (Fig. 3). The polyene chain and the β-ionone ring are within 3.6 Å from the side chains of Trp86, Thr89, Thr90, Met118, Trp138, Ser141, Thr142, Met145, Trp182, Tyr185, Trp189, and Asp212. Site-specific mutagenesis of many of these residues results in changed absorption maxima or a changed rate of thermal isomerization [45–49]. The side chain of Leu93, a residue that influences the rate of thermal 13-*cis* to

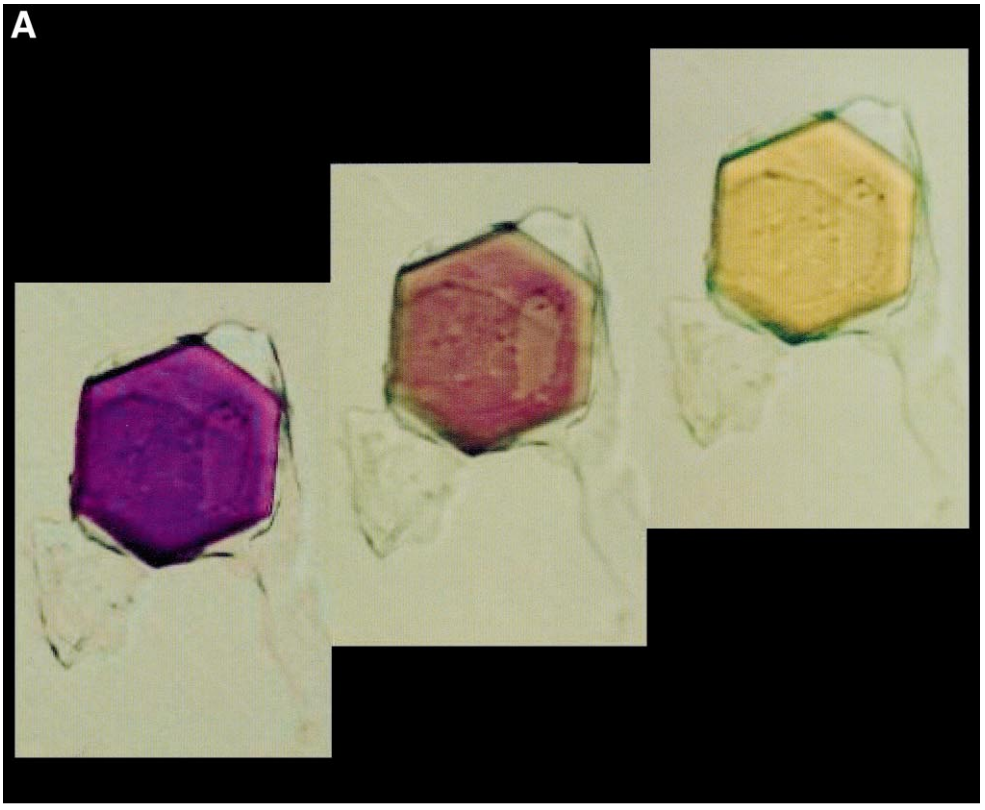
A

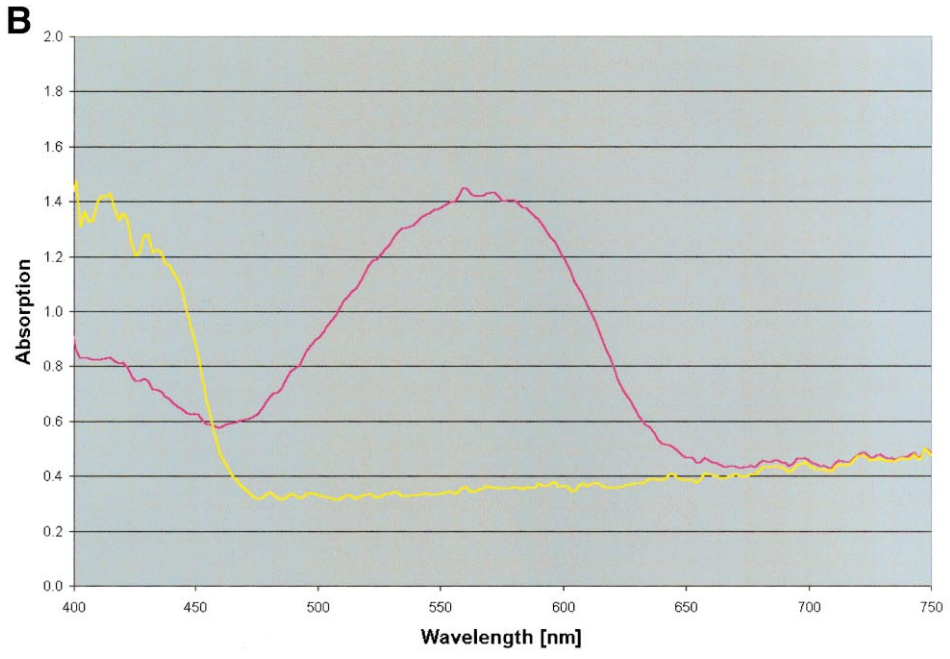
B
Absorption
2.0
1.8
1.6
1.4
1.2
1.0
0.8
0.6
0.4
0.2
0.0
400
450
500
550
600
650
700
750
Wavelength [nm]

all-*trans* reisomerization in the photocycle [50], is within 3.7 Å of the 13-methyl group of the retinal. From linear dichroic measurements the angle between the transition moments of the $N \rightarrow C_5$ and the $N \rightarrow H$ vectors was found to be 70° [51]. In the 1.55 Å structure this angle is 75°. Furthermore, the angle between the retinal chain and the plane of the bilayer had been determined to be 21° for the ground state by polarized FTIR difference spectroscopy [52], in excellent agreement with the 1.55 Å structure where it is 22.5°. For independent determinations of retinal and active site conformations see also the articles by Heyn et al. and Herzfeld et al. in this issue.

Fig. 3 also shows water molecule 401 near the protonated retinal Schiff base, as described by Luecke et al. [13,14]. The presence of bound water near the negatively charged carboxylates of Asp85 and Asp212 had been suggested earlier by the effects of mutations of these residues on the frequency shifts of O–H stretch bands during the photocycle [53–55]. The hydrogen-bonded network, which comprises the positively charged Schiff base, three water molecules (W401, W402, and W406), as well as Asp85 and Asp212, stabilizes the separated charges at the active site in the ground state. Asp85 is kept anionic by additional hydrogen bonding of its OD2 to the OH of Thr89, and Asp212 by hydrogen bonding of OD1 and OD2 to the phenolic OH of Tyr57 and Tyr185, respectively, as well as another hydrogen bond of OD1 to W406 that connects it to the positively charged Arg82. Disruption of the electrostatic balance of this region upon all-*trans* to 13-*cis* photoisomerization of the retinal will destabilize the active site and cause protonation of one of the negatively charged carboxylic acids (Asp85) as well as deprotonation of the Schiff base. The stabilization of the anionic form of Asp212 by hydrogen bonding with the sterically restricted tyrosines ensures that Asp85, rather than Asp212, is the proton acceptor in this first and critical event in ion transport.

3.1.2. The extracellular side

As shown in Fig. 6A, the Schiff base is connected to Arg82 and further to the extracellular surface by an extensive three-dimensional hydrogen-bonded network. Most participants in this network were identified in the earlier 2.3 Å structure [13], but at 1.55 Å resolution four additional ordered water molecules (W404, W405, W406 and W407) became evident [14]. The Schiff base is linked to Arg82 by a continuous hydrogen-bonded chain comprising W402–OD1 of Asp85–W401–W406–NH2 of Arg82. A second chain, comprising W402–OD1 of Asp212–OH of Tyr57–W407, leads to NH1 and NH2 of Arg82. The orientation of the Arg82 side chain connects it to Asp85 via two water molecules (Fig. 6A), and accounts for the observation that the pK_a of Asp85 is increased by 4.5 pH units in the R82Q and R82A mutants [56,57]. Arg82 is connected to the extracellular membrane surface by a network comprising W403–W404–OE1 of Glu194–OE2 of Glu194–OE1 of Glu204–OE2 of Glu204–OH of Ser193, stabilized additionally by water molecule 405. Water molecules 404 and 405 are stabilized by hydrogen bonding with the peptide NH and C=O groups of Tyr79.

The proton release complex is well insulated from the aqueous medium. The region that contains water molecules 403, 404, and 405, together with Glu194 and Glu204, is shielded from the extracellular aqueous interface by Ile78 and Leu201. At the C-terminal end of helix D a buried, unpaired arginine (Arg134) is located near Glu194. The positively charged guanidinium of Arg134 interacts with three peptide carbonyls from residues 126, 128, and 194. This region

←

Fig. 2. Crystal of the bacteriorhodopsin D96N mutant grown in cubic lipid phase and its visible absorption spectra with varying illumination. The crystals form thin hexagonal plates typically about $80 \times 80 \times 15$ μm and are strongly merohedrally twinned along the thin dimension (crystallographic *c*-axis), likely due to macroscopic twinning. (A) The same crystal is shown in three panels: in the left panel fully light-adapted (white light illumination, ground state), in the center panel during dim yellow light ($\lambda > 520$ nm) illumination, in the right panel fully bleached in the M state after illumination with bright yellow light. (B) Two absorption spectra of the crystal as shown in the left panel (purple, light-adapted ground state, $\lambda_{max} = 570$ nm) and the right panel (pale yellow, M state, $\lambda_{max} = 412$ nm). The complete loss of absorption at 570 nm, coupled with the appearance of absorption below 450 nm indicates that no residual ground state remained after illumination with yellow light.

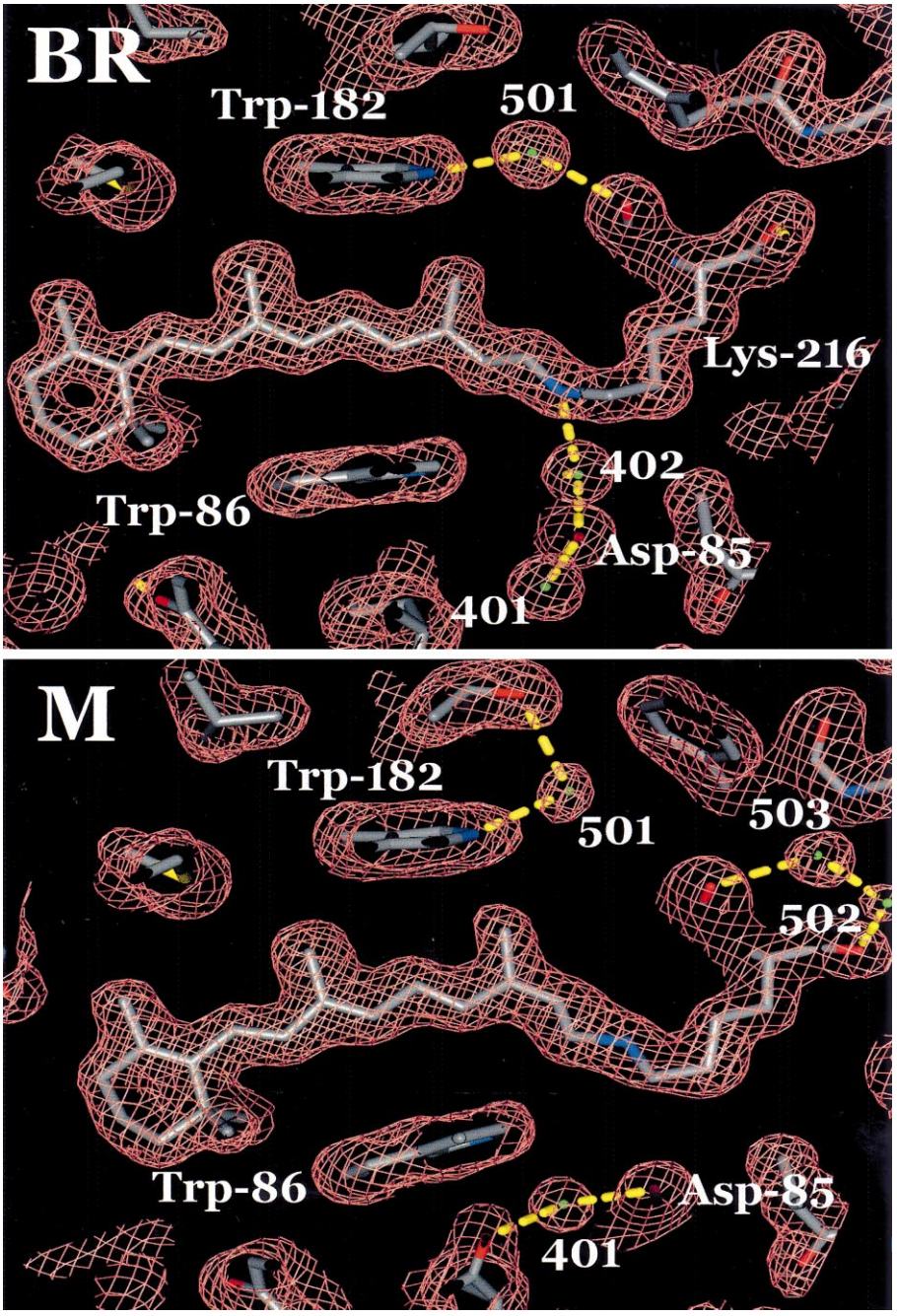

Fig. 3. Electron density maps ($2F_o-F_c$) of the region of the active site contoured at 1σ. (BR) Ground state E204Q structure showing the all-*trans* retinal including the protonated Schiff base and water molecule 402 which is tightly hydrogen-bonded between the protonated, positively charged Schiff base and the anionic carboxylates of the initial proton acceptor, Asp85, and Asp212 (not shown). On the cytoplasmic side (top), water 501 is bridging the indole nitrogen of Trp182 and the peptide carbonyl of residue 215, which due to the local π-bulge in helix G is not participating in helical peptide hydrogen bonding [14]. (M) Early M state from 204Q mutant showing 13-*cis* retinal with kink due to light-induced isomerization [85]. Water 402 is no longer present. In order to accommodate the 13-*cis* configuration, the retinal C_{13}-methyl group has begun to displace the side chain of Trp182 upwards along with water 501, breaking the connection between Trp182 and helix G. Equally significantly, the covalently linked Lys216 chain and nearby π-bulge undergo large conformational changes.

is shielded from the bulk solvent by the aromatic side chain of Phe71.

3.1.3. The cytoplasmic side and a π-bulge-induced kink in the middle of helix G

On the cytoplasmic side, the 1.55 Å structure reveals that transmembrane helix G contains a kink that results from a π-bulge at residue 215. This causes the peptide plane between Ala215 and Lys216 to tilt away from the helix axis, and locally disrupts the α-helical hydrogen bonding pattern. Thus, the carbonyl of residue 213 hydrogen bonds with the amide of residue 218, and the carbonyl of residue 214 interacts with the amide of residue 219. The peptide carbonyl of Ala215 does not participate in backbone hydrogen bonding but instead accepts a hydrogen bond from water molecule W501 (Fig. 3). W501 in turn forms a hydrogen bond with the indole nitrogen of Trp182, a residue in van der Waals contact with the polyene chain of the retinal. The α-helical structure of helix G resumes on the cytoplasmic side of the π-bulge, but in a direction about 15° tilted away from the center. This results in the outward displacement of the C-terminal portion of helix G (residues 222–225) by nearly one helix diameter when compared to a model α-helix aligned with the N-terminal portion of helix G [14].

Such π-bulges within α-helices have been observed relatively infrequently [58], and appear to play mostly structural rather than directly functional roles. However, local weakening of the main chain region around residues 215 and 216 was postulated to play a role in the photocycle [14].

Further stabilization of this disrupted region is provided by a second water molecule, W502, which bridges the carbonyl of the residue to which the retinal is attached via a Schiff base linkage, Lys216, to the carbonyl of Thr46 of helix B (Fig. 6B). Water 502 is located between the Schiff base and Asp96, 5.0 Å from Asp96, and 7.8 Å from the Schiff base in the all-*trans* retinal conformation, making it a prime candidate for participation in proton conduction when the Schiff base is reprotonated by Asp96 during the photocycle. The Schiff base and the carboxyl side chain of Asp96 are 11 Å apart, clearly necessitating one or more carriers for ion transfer.

Through these hydrogen bonds helix G is linked to functionally important regions including the $C_{13}=C_{14}$ double bond of the retinal chain and Asp96. Thus the structure provides the means for mutual interaction of the conformation of the main chain of helix G with the isomeric state of the retinal and the proton affinity (pK_a) of Asp96. This may mediate the observed linkage of the reisomerization of retinal to all-*trans* and the reprotonation of Asp96 from the cytoplasmic surface during the photocycle [1,59,60]. Subsequent rearrangement of water molecules in this region is likely to contribute also to the required lowering of the high pK_a of Asp96 during the photocycle [61]. The high pK_a in the ground state is maintained by the hydrophobic residues Ile45, Leu223, and Leu224 that form the sides of a barrel around Asp96, with lids provided by Phe42, Leu99, and Leu100 from the cytoplasmic side, and by Val49, Leu93, and Phe219 from the direction of the retinal Schiff base.

3.1.4. The lipid bilayer and temperature factors

Bacteriorhodopsin in the purple membrane interacts with specific archaeal lipids that influence the thermal steps of the photochemical cycle [62]. Previous studies have provided some information on bacteriorhodopsin–lipid interaction in two-dimensional and three-dimensional crystals [31,41]. During refinement numerous well-defined difference density features were noted in the form of long narrow cylinders oriented parallel to the crystallographic *c*-axis. From these features 18 lipid chains were identified. Four of these are shorter than full-length because of lack of contiguous electron density. Four individual pairs of full-length chains could be linked with a glycerol backbone, thereby identifying four diether lipids. Lipid head group densities were observed in several instances but were not modeled because of their lower quality and ambiguity. The fact that diether lipids were observed and numerous phytanyl methyl groups could be modeled indicates that native purple membrane lipids [63] were carried along through the detergent extraction of bacteriorhodopsin since only mono-olein, an unbranched monoacyl lipid, was used in preparing the cubic lipid phase. Mass spectrometry of dissolved crystals confirms the presence of major archaeal lipids (unpublished data and [44]).

The lipids form a bilayer in the spaces between adjoining monomers and trimers (Fig. 4). Nearly

all space between the monomers in the *a*/*b* plane is taken up by ordered lipids. The average B factor for lipid atoms is 57 Å^2, as compared to 26 Å^2 for protein atoms, reflecting their higher thermal motion. Since lipid bilayers are naturally fluid systems, their thermal disorder is likely to be higher than that of the associated protein, even when restricted by a crystal lattice. The center of the bilayer is offset by 5 Å from the center of the bacteriorhodopsin molecule toward the extracellular side. Consequently, the cytoplasmic part of the protein is considerably less buried in lipids than the extracellular part and thus shows higher B factors (Fig. 4). This may be relevant to the fact that the cytoplasmic portion, but not the extracellular portion of the protein undergoes large-scale conformational change during the photochemical cycle [64,65]. Similar conformational changes, described as rigid-body motions of the same transmembrane helices as in bacteriorhodopsin, have been detected by spin–spin distance measurements also in visual rhodopsin [66].

The compact arrangement in the *a*/*b* crystallographic plane is identical to the biologically relevant purple membrane (PM) sheets that also form a p3 lattice with $a = b = 61$ Å [30]. Trimer formation from monomers disregarding lipids results in a buried surface area [67] of 13.9%, a fraction that increases only slightly for trimers in PM, demonstrating minimal direct contact between the individual trimers in the bilayer plane. This implies that crystal contacts in the bilayer plane are almost exclusively mediated by lipid molecules that fill the cavities between molecules. The buried surface area of each trimer when lipids are included increases to 14 632 Å^2, or 54.7% (Table 2). The center of the trimer contains two lipids (LIP608 and LIP618) per monomer which cover 8.1% of the protein surface. The remaining lipids form an annulus around the external surface of the trimer. The section of the protein that is buried in the bilayer is more compact and rigid than the solvent-exposed part. On the hydrophobic protein surface, grooves are formed by specific arrangements of the side chains. Whether they are straight or bent, the lipid chains are aligned with these grooves throughout, implying specific interactions between the lipid chains and the protein surface. Theoretical models have predicted such close lipid–protein contacts based on van der Waals–London forces [68].

Most of the lipid tails are relatively straight, but SQU701 adopts a pronounced S-shape, clearly evident in the electron density maps prior to lipid model building. This feature was modeled as a squalene molecule and is located near the middle of the bilayer, and tightly associated with the protein surface where a complementary groove, formed by the side chains of Leu19, Leu22, Val210, Val213, Val217, Leu221, as well as by Ser214 hydrogen-bonded to the peptide C=O of Val210, exists near the π-bulge of helix G. Squalene is present in purple membranes in equimolar amount to bacteriorhodopsin [69]. Its location at the distorted region of helix G is consistent with the observation that squalene strongly affects photocycle reactions [62].

3.2. The late M intermediate

The first high-resolution photocycle intermediate structure to be published was that of the late M intermediate [70]. It was obtained by cryo-trapping of a photostationary state during yellow light illumination of crystals of the D96N mutant. Mutating residue 96 from Asp to Asn dramatically slows down decay of the M state because the Schiff base, instead of being reprotonated from Asp96, now only reprotonates after capturing a proton all the way from the cytoplasmic surface (Fig. 1). The D96N crystals became pale yellow after less than 1 s of illumination with yellow light (Fig. 2A), indicating virtually complete conversion to the M state. Comparison of visible spectra recorded from cryo-cooled crystals of the ground and M state of this mutant confirmed complete conversion to the M state.

3.2.1. Structure of the D96N mutant in the ground state

Virtually no differences between the ground state (light-adapted) form of the D96N mutant and the wild-type protein were detected, except at the location of the residue change. The hydrogen bond between the carboxyl oxygen of the protonated Asp96 and the hydroxyl of Thr46 in the wild type is replaced by a new water, 504, that bridges ND2 of Asn96 and OG1 of Thr46. A structural role for residue 96 in the ground state, implied by these results, is not evident from electron diffraction of D96N at 3 Å resolution [71], but was anticipated from a struc-

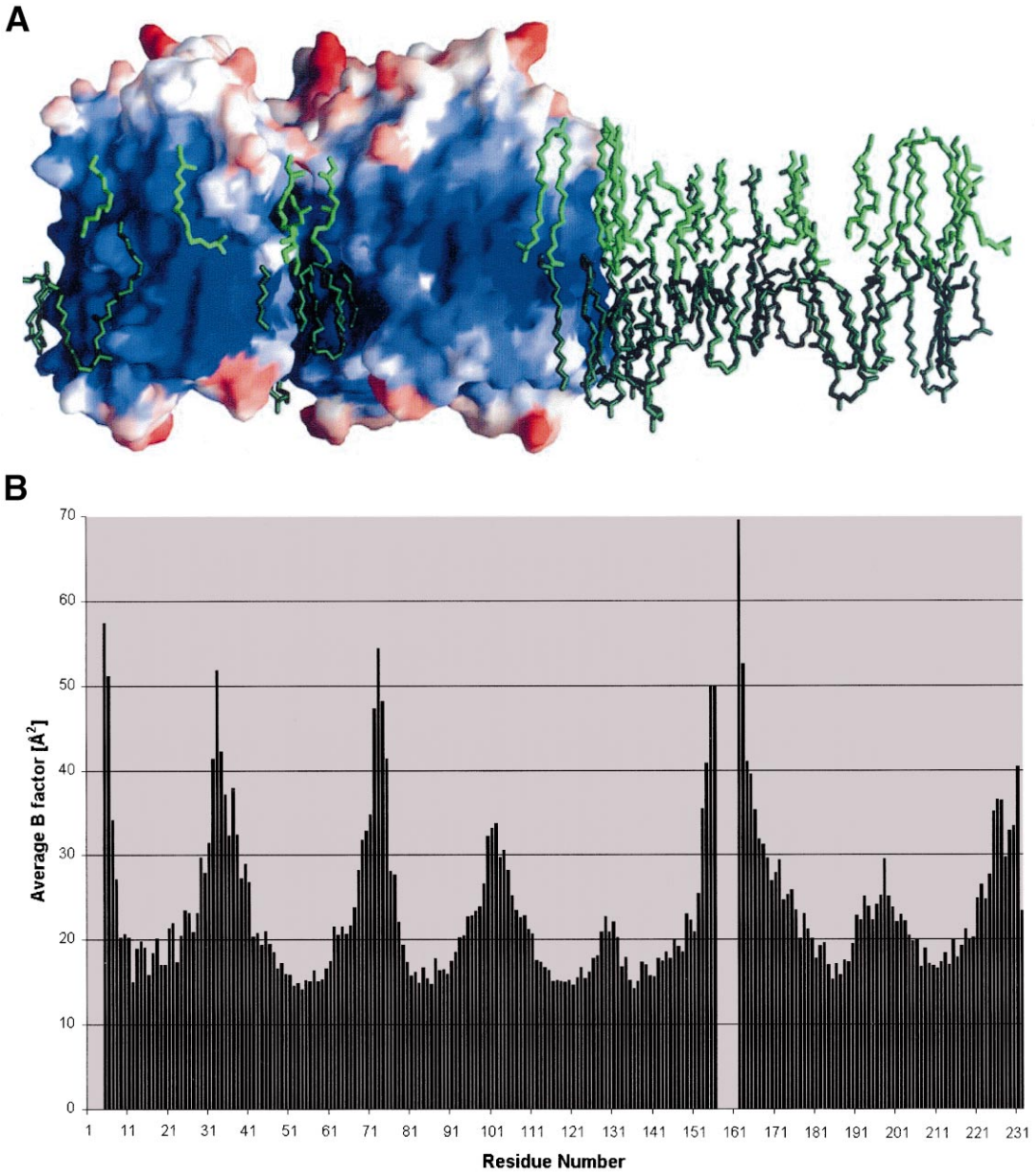

Fig. 4. Refined temperature factors and ordered lipid chains. (A) The transmembrane protein is surface-colored according to refined temperature factors (blue lower, red higher). The ordered lipid chains (green) are arranged in a bilayer with the upper leaflet colored in light green and the lower leaflet in dark green. The bilayer is in the crystallographic *a-b* plane which obeys the same p3 symmetry as the naturally occurring two-dimensional purple membrane crystals. Note that bacteriorhodopsin is not symmetrically embedded in the bilayer; the cytoplasmic side (top) projects further from the bilayer surface and displays higher temperature factors than the extracellular side (bottom). This asymmetric arrangement, if preserved in other seven transmembrane helical proteins, might be necessary for the observed large conformational changes in the cytoplasmic loops during G protein-coupled receptor signaling. Viewed from above, the lipids form a tightly packed annulus round the trimeric bacteriorhodopsin units (not shown) which is responsible for the crystalline order in the *a-b* plane. (B) Plot of the average refined temperature factor of the main-chain atoms vs. residue number. The B factors are lowest in the center of the bilayer (less than 20 $Å^2$) and highest for the loop regions. The four residues at positions 157–161 are not modeled [14].

tural difference between the D85N and D85N/D96N mutants [72].

3.2.2. Retinal binding pocket and the active site

According to overwhelming evidence from resonance Raman and NMR spectra, the configuration of the retinal in the M state is 13-*cis*,15-*anti*. The disposition of the polyene chain and its changes in M, as well as its angle to the membrane plane and its changes have been estimated from transient linear dichroism in the visible and the infrared during the photocycle [73]. Earnest et al. reported the angles between the conjugated π system of the retinal and the bilayer plane in the ground and M states to be 21° and 28°, respectively [52]. The positions of the ring and the 13-methyl group in the ground state have been determined with neutron diffraction of protein with specifically deuterated retinals [74]. The X-ray crystal structure of the cryo-trapped late M intermediate clearly shows that the retinal indeed assumes the 13-*cis*,15-*anti* configuration. The kinking of the *cis*-retinal moves the polyene chain between C_{10} and the Schiff base nitrogen towards the cytoplasmic side. The largest relative movement is for C_{14} which is displaced by 1.7 Å. The 13-methyl group moves by 1.3 Å toward the cytoplasmic side. In comparison, the movement of the β-ionone ring, by 0.4 Å towards the Schiff base, is relatively minor. The measured angles between the conjugated π system of the retinal and bilayer plane for the BR and M states are 20.2° and 29.6°, respectively, in excellent agreement with the polarized infrared results [52]. For independent determinations of retinal and active site conformations see also the articles by Heyn et al. and Herzfeld et al. in this issue.

In response to the photo-induced retinal isomerization, the entire active site undergoes considerable rearrangement. The retinylidene nitrogen moves toward the cytoplasmic side by 0.9 Å and its electron pair turns away from Asp85. The OD1 of Asp85 is now 1.2 Å farther away from the Schiff base nitrogen. Either because of the isomerization of the retinal, or because of the proton transfer that follows it, water molecules 401, 402 and 406 are replaced by a single water, that is positioned 1.9 Å from water 401 in the ground state and now occupies a position near the center of gravity of the former three water molecules (Figs. 3 and 6). The protonated Asp85 has lost all its former hydrogen bonding partners, except water 401, while Asp212 retains its connection to the phenolic OH groups of Tyr185 and Tyr57, and forms a new hydrogen bond to water 401 and to the previously unsatisfied indole nitrogen of Trp86.

The main chain and side chain of Lys216 move, with the α-carbon accommodating the *cis*-retinal kink by a 1 Å motion in the extracellular direction. The side chain of Trp182 is displaced by 1.5 Å in the cytoplasmic direction because of its proximity to the 13-methyl group, resulting in breaking the water-mediated connection between Trp182 and the carbonyl of residue 215 (Fig. 6). The side chain of Leu93, also near the 13-methyl, is rotated by about 90° (χ_1 by −26°, χ_2 by −65°). Trp86, on the extracellular side of the retinal, tilts toward the polyene chain that has moved away from it. Residues that contact the β-ionone ring, Trp138, Ser141, and Met145, are moved much less, consistent with its lesser displacement. It appears, therefore, that the steric conflict that develops upon the rotation of the $C_{13}=C_{14}$ double bond between the retinal chain and the protein involves primarily the 13-methyl group and the side chains of three residues that make contact with it and with the retinal chain. The slowing of thermal reisomerization of the retinal during the photocycle in mutants of Leu93 [27,75], as well as in W182F [48], had suggested such an interaction.

In late M the measured pK_a of the Schiff base is greatly lowered [76], and it has been assumed that this is largely because the retinylidene nitrogen is displaced into a highly hydrophobic region by isomerization of the retinal. The structure confirms that this is indeed the case. The cytoplasmic side that the Schiff base faces in M shows no ordered waters and is strongly hydrophobic in character due to the side chains of Leu93 and Val49. Likewise, there are drastic changes around Asp85 that account for the proposed [77–79] greatly increased pK_a of this residue. Two of its three previous hydrogen bonds are lost, and in the third, to water 401, the carboxyl oxygen of Asp85 could now be the proton donor, further stabilizing its protonated state. The structure near Asp85 (Fig. 6B) is consistent with dehydration as the cause of the high frequency of the protonated carboxyl stretch of this residue [79].

3.2.3. The extracellular side

Toward the extracellular side, a three-dimensional network of hydrogen-bonded side chains and water leads from the active site of the ground state (Asp85) to the residues that participate in the release of a proton to the extracellular surface upon protonation (Arg82, Glu194, and Glu204, Fig. 6A). One continuous chain is through water 406 which connects both Asp85 (through waters 401 and 406), and Asp212 (through water 406), to NH1 of Arg82 [14]. A second chain, from Asp85 to both NH1 and NH2 of Arg82, in the ground state is through water 402, Asp212, Tyr57 and water 407. Both chains are fragmented in M because waters 402 and 406 are absent and the side chain of Arg82 moves downward (CZ is displaced by 1.6 Å along the *z* axis, Fig. 6B).

In the ground state NH1 and NE of Arg82 are both connected to Glu194, through water molecules 403 and 404, while the side chain oxygens of Glu194 and Glu204 form a direct hydrogen bond, presumably via a shared proton [14,41]. In M, Glu194 retains its connection only with the NE of Arg82. The connection between Glu194 and Glu204 is now through water 404 (Fig. 6). Loss of the direct hydrogen bond between Glu194 and Glu204 in the M state would be expected if the source of the released proton were a proton shared between Glu194 and Glu204 [14,41], or either Glu204 or Glu194. Indeed, the positive charge of Arg82 is now closer to the two glutamates, and would stabilize them if they were both anions after release of the proton to the extracellular surface.

3.2.4. The cytoplasmic side

Low resolution (≥ 3 Å) diffraction difference maps in projection [71,80], and cryo-electron microscopy of tilted samples [64], had indicated that large structural changes occur in the cytoplasmic (but not the extracellular) region of the protein in the M and N intermediates. The most prominent of these are the tilt of the cytoplasmic end of helix F away from the center of the protein, and an increase of density of uncertain origin at helix G. These two helices are strongly and uniquely affected in the M state. From the electron density maps and the refined temperature factors of main chain atoms it is clear that the cytoplasmic ends of helices F and G are disordered between the E–F interhelical loop and residue 176, and beyond residue 222, respectively. This is unlike the ground state of D96N, where these regions could be modeled as far as to the surface as residues 162 and 231, respectively [70]. In the region where the temperature factors were low enough to allow modeling, notable RMS deviations between the ground and M states of D96N could be seen in helix G, but not in helix F with the exception of the two residues nearest its disordered segment. The movement of the main chain at these two residues is away from the center of the molecule as concluded earlier from projection difference maps [64,65,71,80], with the α-carbon of the first residue to move, Val177, displaced by 1.6 Å. The tilt in this M state involves therefore only the segment between residues 162 and 177, rather than the entire cytoplasmic half of helix F, with Tyr185 and Pro186 acting as hinge as was often assumed. The position of the ring of Tyr185 also remains virtually unchanged in M. No major displacements of the main chain are evident in helices A–E.

The main chain movements within helix G involve the local region around Ala215 and Lys216, where the π-bulge was described [14]. The peptide carbonyl of 215, which in the ground state is tilted outward and away from the helix axis, is now aligned with the helix axis. In contrast, the peptide of carbonyl 216, which in the ground state accepts a hydrogen bond from amide 220, is now tilted away, resulting in a loss of the α-helical hydrogen bond. These local conformational changes of the π-bulge are likely to be a direct consequence of the strain induced by isomerization of the covalently linked retinal.

The barrier to proton conduction in the cytoplasmic region at this point in the photocycle must be due to a lack of polar residues capable of proton transport, coupled with a constellation of hydrophobic residues that occlude the interhelical region. The side chains of the most prominent of these hydrophobic residues, Leu93 and Phe219, rotate away so as to provide the possibility of a pathway between the surface and the Schiff base. Unlike in the wild type, the very slow decay of the M state of the D96N (at pH 7, τ is tens of seconds) is limited by proton uptake at the surface [81–83], and its greatly increased entropic barrier was suggested to reflect a structural requirement for capturing the proton from the bulk [81]. Presumably, M decay occurs

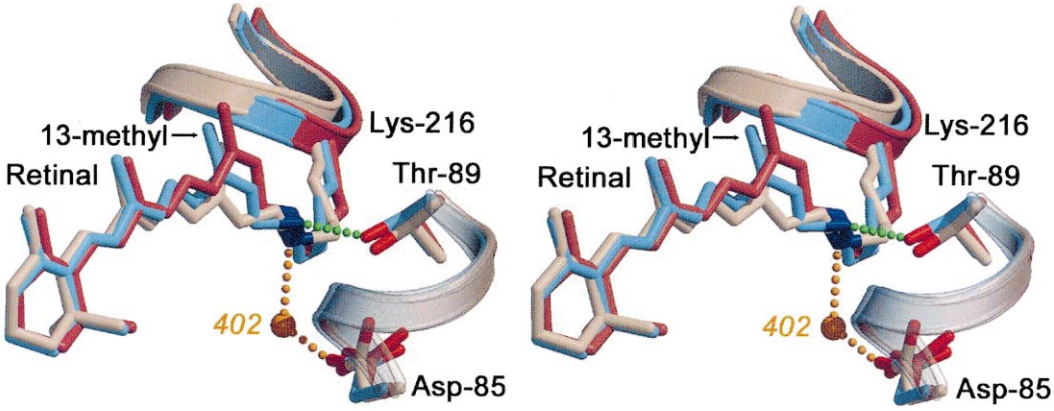

Fig. 5. Stereo representation showing the progressive light-induced conformational changes in the retinal region from the ground state (colored beige), to the early M state (colored blue, E204Q mutant), and to the late M state (colored red, D96N mutant). The hydrogen bond between the Schiff base and water 402 which is present only in the ground state is shown in gold, and the hydrogen bond between the deprotonated Schiff base and Thr89 in the early M state is shown in green.

when either hydrogen bonding groups (of necessity, water molecules) form a transient proton-conducting network from the surface to the Schiff base, or mobile water molecule(s) carry a proton through a transient pathway. This structural transition will not yet have taken place in M, although the disorder of the cytoplasmic ends of helices F and G hint at conformational changes that make the region above Asn96 more permeable to water.

3.3. Other intermediates

3.3.1. A low-temperature K intermediate

Shortly after publication of the late M intermediate structure, the 2.1 Å structure of a low-temperature K intermediate obtained by continuous illumination with green light (532 nm) at 110 K (denoted K_{LT}) was reported [84]. The study determined 35% occupancy for the K_{LT} state, with the balance assumed to be ground state. Analysis showed a diminishing of the electron density at the ground state position of water 402, coupled with a mutual approach of the carboxylates of Asp85 and Asp212, as well as the beginning of a locally disrupted hydrogen bonding network at residue 216 in helix G.

Spectroscopy indicates that the retinal is not relaxed in the K state [18–20]. However, due to lack of detailed information in this K_{LT} study, the retinal was restricted to a planar 13-*cis*,15-*anti* geometry with the protonated Schiff base pointing toward the cytoplasmic side [84]. The implications of this orientation for the mechanism of the early steps in the photocycle will be discussed in Section 4.

3.3.2. An early M intermediate

Very recently, we determined the structure of the M state produced in a photostationary state of the E204Q mutant [85]. This mutant blocks proton re-

→

Fig. 6. Stereo views of the structure and hydrogen bonding region in the ground state (A) and the M state (B). The M state view is a composite comprised of the retinal region and cytoplasmic side (top and center) of the early M structure (where the E204Q mutation has minimal effects) and the extracellular side (bottom) of the late M structure (where the D96N mutation has minimal effects). The extensive hydrogen bonding network leading to the extracellular surface found in the ground state is fragmented in the M state. Specifically, waters 402 and 406 are lost, new hydrogen bonds are formed between Trp86 NE and Asp212 OD1, and between Tyr83 OH and Glu194 OE1; the now protonated carboxylate side chain of Asp85 has lost hydrogen bonds from water 402 and Thr89 OH; the guanidinium moiety of Arg82 has moved away from the Schiff base and toward the extracellular side (downward). In contrast, the very apolar cytoplasmic region between Asp96 and the Schiff base in the ground state is starting to show an ordered network of water molecules (W504, W503, W502), forming a chain from the proton donor in the M to N reaction, Asp96, to the carbonyls of residues 215 and 216 which are within 5 Å of the deprotonated Schiff base.

lease [86] (Fig. 1, step 2), and we expected that the M state that accumulates in these crystals under yellow light illumination would reflect features of an earlier M state, unlike the late M intermediate produced from D96N crystals. Many of the structural changes observed in the early M are similar, but of lesser magnitude than those in the previously determined late M [70].

As in the case of the D96N late M, this M was cryo-trapped after brief (<1 s) illumination at am-

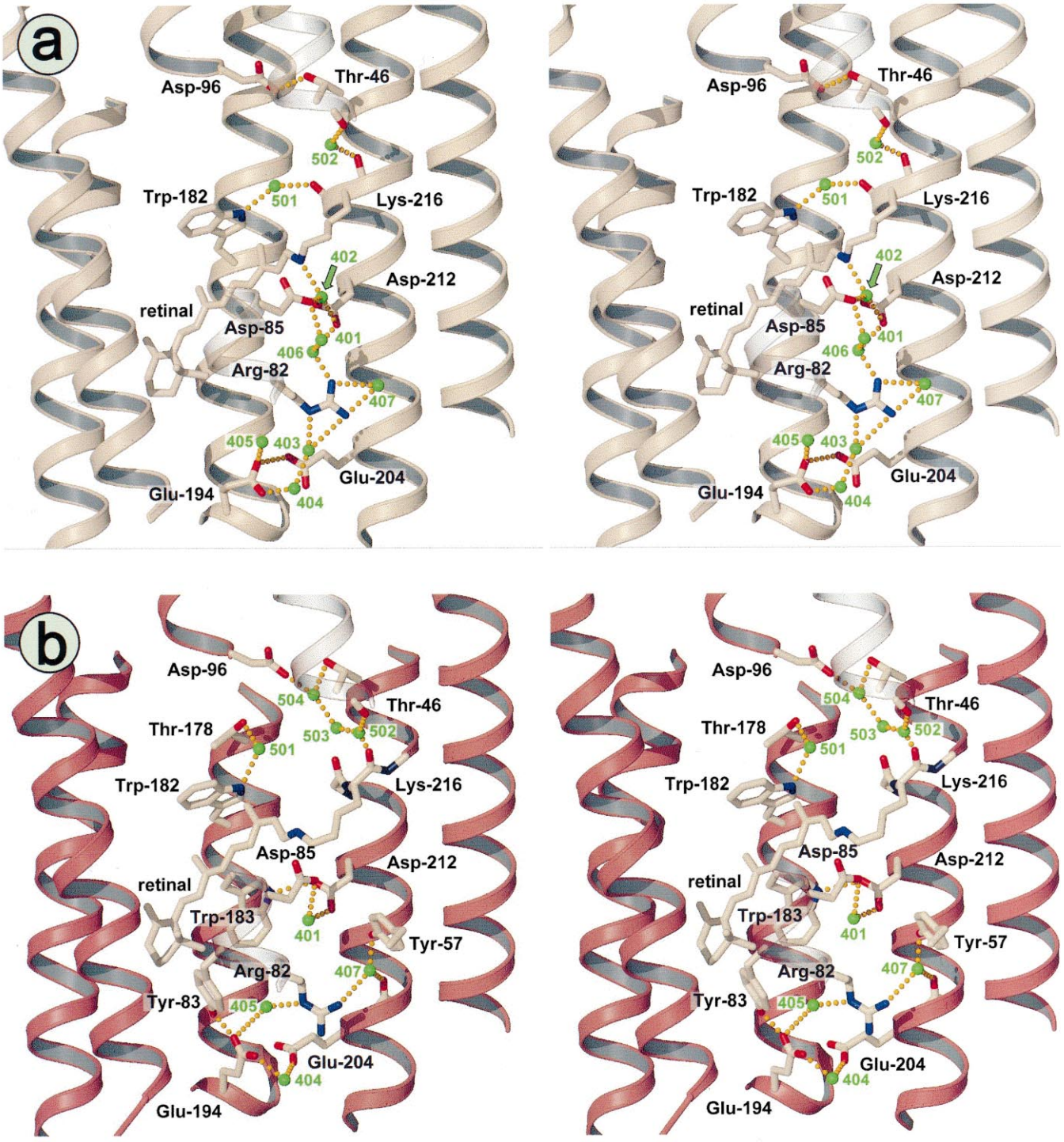

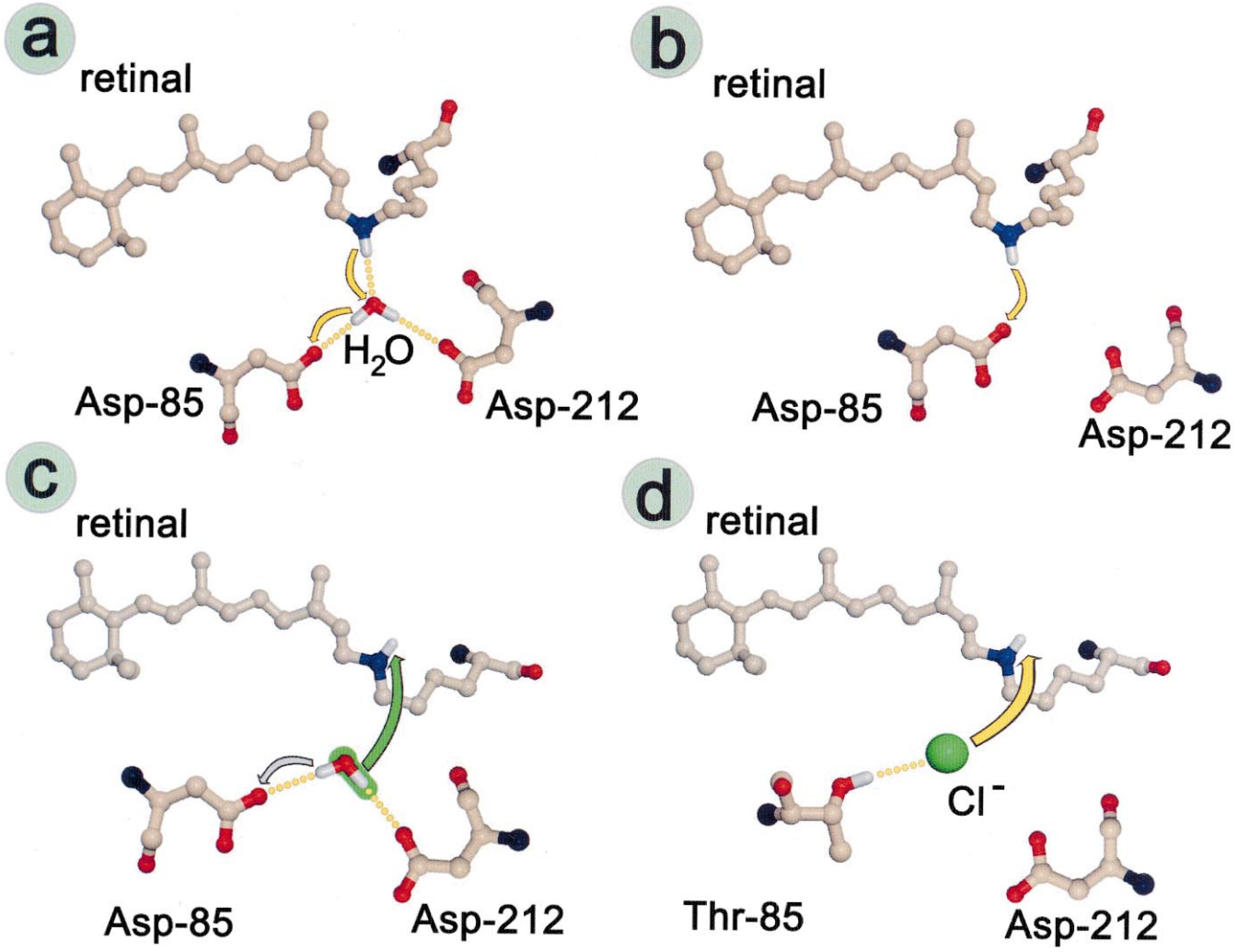

bient temperature. The ground state structure at 1.7 Å resolution reveals that structural rearrangements upon the conservative replacement of a protonated glutamic acid with a glutamine are more extensive than in the case of the D96N mutation [70]. However, all changes are confined to the extracellular side. Furthermore, the M state structure of E204Q is considerably better ordered than the one previously reported for the M state of the D96N mutant, in particular the cytoplasmic ends of helices F and G [70]. The increase in resolution from 2.0 Å for the late M structure to 1.8 Å for the early M intermediate is accompanied by dramatically improved electron density maps (Fig. 3) in which new water molecules could be localized. The crystallographic R factors are also much improved.

Fig. 3 shows density maps of the region of the retinal, Asp85, and other neighboring residues in the ground and M states of the E204Q mutant. The rotation of the C13=C14 double bond, and lack of rotation of the C14–C15 single bond and the C15=N double bond are all evident, as expected for the 13-*cis*,15-*anti* configuration. Also noted are the changed hydrogen bonding of water molecule 501, the absence of water 402, and the appearance of water 503 in the M state.

The Schiff base nitrogen is displaced by 0.6 and 0.9 Å, and the CE of the connected Lys216 chain by 1.3 and 1.1 Å, in the early and late M states, respectively (Fig. 5). Already in the early M state, a rotation around the CB–CG bond of Asp85 moves OD2 and OD1 relative to both the Schiff base NZ, and OG1 of Thr89 to which Asp85 is hydrogen-bonded in the ground state. OD1, in particular, which is

Fig. 7. Three mechanistic models of the early events in the photocycle leading to deprotonation of the Schiff base and protonation of Asp85 (L to M reaction) and a comparison with a proposed chloride (Cl^-) pumping model for halorhodopsin and the D85S/T mutant of bacteriorhodopsin. (A) Water 402 is still bridging the Schiff base and Asp85. This scenario would imply an L state retinal with large deviations from the relaxed 13-*cis*,15-*anti* conformation, which could be achieved by counter-rotations around the $C_{13}=C_{14}$, C_{14}–C_{15} and/or the $C_{15}=N$ bonds to point the Schiff base proton toward the extracellular side. For simplicity, this figure is drawn with a pure $C_{15}=N$ counter-rotation similar to dark-adapted (13-*cis*,15-*syn*) retinal. In a concerted reaction, water 402 would lose a proton to Asp85 while receiving the Schiff base proton. Subsequently, the retinal could relax into a less strained 13-*cis*,15-*anti* configuration. (B) A variation of model A without water 402 present. This model involves a close approach of the Asp85 carboxylate to the protonated Schiff base for direct proton transfer. As in the case of model A, severe torsional strain of the retinal bonds between C_{13} and the Schiff base nitrogen would be necessary to continue pointing the Schiff base proton towards the extracellular side in spite of the 13-*cis* conformation of the retinal. (C) Novel model of bacteriorhodopsin as a net hydroxide (OH^-) pump from the extracellular to the cytoplasmic side, instead of the commonly assumed pumping on protons (H^+) in the opposite direction. This model is mainly based on the presence of water 402 in a key position in the ground state structure (Figs. 3A, 5 and 6) [13,14] and its absence in both M structures (Figs. 3B, 5 and 6) [70,85]. The light-driven *all*-trans to 13-*cis*,15-*anti* isomerization of the retinal in the BR to K transition generates significant electrostatic conflict for the anionic pair of Asp85 and Asp212 by displacing the positively charged Schiff base away from the pair and by reorienting the Schiff base proton towards the very apolar cytoplasmic region. In the hydroxide pumping model this conflict would be resolved by a concerted sequence of events: (1) The anionic aspartates display sharply elevated pK_as (proton affinities). Nearby water 402, already highly polarized by being located between three formal charges, loses a proton to Asp85, generating a hydroxide ion (OH^-). (2) This newly created mobile hydroxide anion would be attracted by the Schiff base cation on the cytoplasmic side of the retinal. (3) The OH^- would move to the cytoplasmic side and due to its basicity (proton affinity) immediately abstract the proton from the Schiff base to yield a deprotonated Schiff base (M state) and a water. (D) A model for chloride (Cl^-) pumping by the D85S/T mutant of bacteriorhodopsin and the naturally occurring chloride pump halorhodopsin [5,6]. Note the analogy to the hydroxide pumping model in C. Due to the replacement of one anionic aspartate immediately below the Schiff base (Asp85) with a neutral hydroxyl moiety, the weak base chloride now replaces water 402 between the positively charged Schiff base and Thr85 in the ground state. Upon light-induced isomerization of the retinal the chloride anion (analogous to the transiently generated hydroxide anion in model C) would follow the Schiff base to the cytoplasmic side of the retinal. Due to the lower basicity (proton affinity) of the chloride vs. hydroxide, the Schiff base remains protonated throughout this photocycle [5,6].
←

hydrogen-bonded to water 402 (and water 401, not shown) in the ground state, is displaced by 1.6 Å. In both M states waters 402 and 406 are absent. All other changes immediately to the extracellular side of the Schiff base in the early M are the same as described for the late M [70].

On the extracellular side, Arg82 moves toward the proton release complex despite the fact that the E204Q mutant does not show proton release at this point in the photocycle. This suggests that the main event that triggers the side chain motion is the protonation of Asp85 in the L to M reaction. The reported asymmetry between the guanidinium nitrogens of Arg82 in the M state of the wild-type protein by solid-state NMR [87] is consistent with its highly asymmetric environment in the structure of both M intermediates (Fig. 6B).

On the cytoplasmic side, two additional ordered water molecules could be located. A sequence of atomic displacements along a chain that extends from the π-bulge of helix G to Thr46, and repacking of hydrophobic side chains between Trp182 and Asp96, both initiated by conformational changes of the retinal, move the Thr46 hydroxyl and the Asp96 carboxyl apart and allow the intercalation of a water molecule, 504, resulting in the observed lowering of its pK_a. Water 504 is hydrogen-bonded, in turn, to another new water, 503, which is hydrogen-bonded also to water 502 that is present in both M and the ground state (Fig. 6). Waters 504, 503 and 502 are beginning to form a hydrogen-bonded chain from the proton donor in the M to N reaction, Asp96, toward the Schiff base. The functional implications of these waters will be discussed in the next section.

4. Clues to function from structure

With several high-resolution structures of the ground and intermediate states available, a new level of understanding of the prototypical ion pump bacteriorhodopsin can be achieved. Based on the exact positions of ordered (but nevertheless mobile) water molecules in combination with the elucidation of detailed conformational changes of the retinal and protein, we are now in a position to propose very de-

tailed mechanisms for the molecular events in the early part of the photocycle.

A light-driven ion pump must convert the photon energy into a meta-stable conformational state whose subsequent relaxation is coupled to the unidirectional movement of ions. In the case of BR, isomerization of all-*trans* to 13-*cis* retinal could in principle result in two fundamentally different conformations for the L state. One conformation would contain a highly strained 13-*cis* retinal that would maintain a Schiff base N–H orientation toward the extracellular side through severe torsional strain of the bonds between C_{13} and the Schiff base nitrogen. Two mechanisms based on this L conformation are presented below in Section 4.1.1.

Alternatively, the L state could be comprised of a much less twisted 13-*cis*,15-*anti* retinal with a Schiff base orientation toward the cytoplasmic side. Light-induced transfer of the Schiff base N–H from the hydrophilic environment of water 402 and the two aspartic acids 85 and 212 on the extracellular side into the very hydrophobic environment formed by Leu93 and Val49 on the cytoplasmic side would suggest an entirely different mechanism for the initial proton transfer, discussed in Section 4.1.2 below.

4.1. The role of water 402 in the early photocycle

Three alternative mechanisms for the first and crucial ionization change in the bacteriorhodopsin photocycle (the deprotonation of the Schiff base and the protonation of Asp85, Fig. 1, step 1) are presented. These mechanisms attempt to address in detail the question of how the Schiff base becomes deprotonated and Asp85 protonated in the L to M reaction. They are based on the presence of water 402 in the ground state (Figs. 3A,6A), which was first identified in 2.3 Å structure [13], and subsequently confirmed by 1.9 Å [44] and 1.55 Å [14] studies, and its absence in both the early [85] and late M structures [70].

4.1.1. Bacteriorhodopsin as a proton pump

Bacteriorhodopsin is commonly regarded as a light-driven pump that actively translocates protons from the cytoplasmic to the extracellular side. The two mechanistic models of the early events in the photocycle leading to deprotonation of the Schiff base and protonation of Asp85 (L to M reaction) in this section are consistent with net proton pumping. They are based on different assumptions about the position of water 402 in the L state for which no high-resolution structure has been determined to date.

(A) In the first model, water 402 is still bridging the protonated Schiff base and anionic Asp85 in the L state. This scenario would imply a retinal with large deviations from the relaxed 13-*cis*,15-*anti* conformation in the L state, which could be achieved by counter-rotations around the $C_{13}=C_{14}$, C_{14}–C_{15} and/or the $C_{15}=N$ bonds to point the Schiff base proton toward the extracellular side. For simplicity, Fig. 7A depicts a pure $C_{15}=N$ counter-rotation similar to dark-adapted (13-*cis*,15-*syn*) retinal. In this model, water 402 would lose one proton to Asp85 while receiving the Schiff base proton in a concerted reaction. After neutralization of the Schiff base/Asp85 charge pair the retinal could relax into a true 13-*cis*,15-*anti* configuration.

(B) This model is a variation of model A with water 402 no longer present. After loss of water 402 in the early events after photoisomerization, the model postulates a close approach of the Asp85 carboxylate to the protonated Schiff base for direct proton transfer (Fig. 7B). As in the case of model A, severe counter-rotations of the retinal bonds between C_{13} and the Schiff base nitrogen would be necessary to continue pointing the Schiff base proton towards the extracellular side in spite of the 13-*cis* conformation of the retinal. The L to M transition would proceed by direct proton transfer from the Schiff base to Asp85, followed by a relaxation of the unprotonated retinal into 13-*cis*,15-*anti*.

In the scheme of model A it is not apparent why the thermally accessible dark-adapted state with a 13-*cis*,15-*syn* retinal [88,89] would not result in a similar proton transfer reaction. Presumably, retinal strain in the L intermediate in the form of distorted single and double bonds would lead to this different outcome.

The negative difference density at the position of water 402 in the low-temperature K (K_{LT}) structure [84] appears to favor mechanism B. However, neither mechanism A nor B is supported by the retinal conformation selected for the K_{LT} state that arises immediately before the L state for the following reason. Both models require substantial counter-rotations

around the $C_{13}=C_{14}$, C_{14}–C_{15} and/or the $C_{15}=N$ bonds to point the Schiff base proton toward the extracellular side whereas the K_{LT} structure (PDB codes 1QKO/1QKP), for lack of relevant structural information, was modeled as a relaxed 13-*cis*,15-*anti* retinal with the Schiff base pointing toward the cytoplasmic side [84].

4.1.2. Bacteriorhodopsin as a hydroxide pump

The third model presented here postulates that bacteriorhodopsin functions as a net hydroxide (OH^-) pump from the extracellular to the cytoplasmic side instead of the commonly assumed pumping of protons (H^+) in the opposite direction. This model is largely based on the presence of water 402 in a key position in the ground state structure (Figs. 3A,5 and 6) [13,14] and its absence in both M state structures (Figs. 3B,5 and 6) [70,85]. The light-driven all-*trans* to 13-*cis*,15-*anti* isomerization of the retinal in the BR to K transition generates significant electrostatic conflict for the anionic pair of Asp85 and Asp212 [16], by displacing the positively charged Schiff base away from the anion pair and by reorienting the Schiff base proton towards the very apolar cytoplasmic region. In the hydroxide pumping model this conflict would be resolved by the following concerted sequence of events (Fig. 7C):

1. The anionic aspartates Asp85 and Asp212 display sharply elevated pK_as (proton affinity). In this model, nearby water 402, already highly polarized by being located between three formal charges, donates a proton to Asp85, generating a hydroxide ion (OH^-).
2. This newly created mobile hydroxide anion would be repelled by the still anionic Asp212 on the extracellular side and attracted by the Schiff base cation on the cytoplasmic side of the retinal about 4 Å away.
3. The OH^- would move to the cytoplasmic side and, due to its high basicity (proton affinity), immediately abstract the proton from the Schiff base to yield a deprotonated Schiff base (M state) and a water. The general hydrophobicity of the cytoplasmic region would ensure that this proton transfer reaction, which results in two uncharged entities (the unprotonated Schiff base and a water), is virtually irreversible. The net effect of this scenario, taking into account the thermal reisomerization of the reprotonated retinal later in the photocycle, would be the transport of one hydroxide past the retinal, from the extracellular side to the cytoplasmic side.

This mechanism would provide a means for converting the energy stored in the isomerized retinal into a largely electrostatic driving force for ion translocation. Vectoriality would be achieved through irreversible charge separation following the dissociation of water 402 into H^+ and OH^-, and movement of OH^- to the cytoplasmic side. Later events in the photocycle could be facilitated by relaxation of the remaining steric conflicts between the retinal and the active site, in particular with Trp182.

Another attractive feature of this model is the resulting conceptual similarity of bacteriorhodopsin and halorhodopsin. Both proteins would function as anion pumps (Fig. 7D), and the fact that the single-site mutation Asp85 to Ser85 (D85S) turns bacteriorhodopsin into a chloride pump [90,91] could be explained in very simple terms. As a net hydroxide pump, BR would require the net translocation of one hydroxide from the extracellular to the cytoplasmic side per pump cycle. Most reactions that are viewed as pure proton transfers in the older models would now have to be accompanied by a water translocation in the opposite direction. For example, the proton transfer during the Schiff base reprotonation from Asp96 in the M to N reaction (Fig. 1, step 3) would require a concomitant net water movement from the Schiff base to Asp96 in order to yield an overall hydroxide translocation. The observed loss/disordering of water molecules on extracellular side (waters 402 and 406), combined with the appearance/ordering of new waters on cytoplasmic side (waters 503 and 504) in the early M structure is a strong indication of the central role discrete water molecules play in the bacteriorhodopsin photocycle.

The two mechanisms in Section 4.1.1 propose indirect or direct transfer of the Schiff base proton to Asp85 on the extracellular side. In these cases, the energy necessary to drive the L to M reaction would not be due to a photo-induced charge separation. The majority of the energy would have to be derived from the steric and torsional strain of the active site

due to photoisomerization that in turn would modulate the proton affinities of key ionizable groups.

In contrast, the hydroxide pumping model in this section proposes a photo-induced charge separation early in the photocycle (K and L states) which would drive OH^- translocation past the retinal in the L to M reaction. In this context it should be noted that Mitchell's chemiosmotic hypothesis did not rule out OH^- transport in favor of H^+ transport [92].

4.2. The role of other internal waters

In the ground state, the extracellular side displays an extensive hydrogen-bonded network including seven water molecules. In contrast, the scarcity of ordered water molecules on the cytoplasmic side explains why bacteriorhodopsin does not passively conduct ions in the ground state. In the M intermediates, the situation has changed significantly. We observe decreased hydration and a fragmentation of the ordered network on the extracellular side, and at the same time increased hydration on the cytoplasmic side. This shift in hydration offers an explanation for the substantial pK_a changes of Asp85 (increase) and Asp96 (decrease) during M and N states of the photocycle. While by no means conclusive, this shift would be congruent with the movement of water past the retinal during the photocycle.

The water chain forming from Asp96 toward the Schiff base suggests the beginning of a pathway for ion conduction in the otherwise hydrophobic half channel. There is reason to believe that the structures of the photocycle intermediates following the M state will reveal the molecular details of ion transport on the cytoplasmic side.

4.3. The role of arginine 82

The structures of the early and late M intermediates clearly show that pronounced downward motion of the guanidinium moiety of Arg82 is a direct consequence of electrostatic changes at the active side that are leading to the protonation of Asp85 in the L to M transition. This motion of a charged group away from the Schiff base and toward the proton release group affects the pK_as of several ionizable residues, leading to a lowering of the pK_a of the proton release group that results in the release of a proton to the extracellular surface. This mechanism of long-distance electrostatic coupling of the protonation states of Asp85 and the proton release group via movements of the Arg82 side chain explains the importance of this side chain in ion translocation [93].

The last step in the photocycle, the resetting of the pump to the ground state (Fig. 1, step 5), requires transfer of a proton from Asp85 to the proton release group. This proton transfer over a distance of about 13 Å has to involve Arg82, but due to the high pK_a of the guanidinium moiety it is unlikely that the proton transfer involves transient deprotonation of Arg82. In the hydroxide pumping mechanism, in addition to this proton transfer, the translocation of a water from the extracellular surface to replace water 402 between Asp85 and the Schiff base is required. This additional water translocation over more than 15 Å would provide an explanation for the slow rate constant of the O to BR reaction.

5. Future directions

A complete picture of the conformational changes during the bacteriorhodopsin photocycle will require the determination of the high-resolution structures of the K, L, N, and O intermediates. One problem in this endeavor is the fact that all these intermediates can only be obtained at partial occupancies due to spectral overlap with each other and the ground state. Crystallographic analysis of moderate structural changes in these intermediates is far more challenging when carried out with a background of the ground state structure.

The structure of the late M intermediate as obtained from the D96N mutant [70] has serious shortcomings on the cytoplasmic side due to the high degree of disorder encountered. Structural determination of the structure of a late M intermediate with helices F and G ordered all the way to the cytoplasmic surface might provide clues of how the large conformational changes on the cytoplasmic side are brought about. However, crystal packing, specifically the interference of the BC loop of one molecule with the conformational changes at the cytoplasmic surface of a molecule in the next layer of the crystal, might prevent the formation of a homogeneous pho-

tostationary state. This complication might also affect the N and O intermediates.

Of particular interest will be the structure of the L intermediate as this is the conformation immediately preceding the deprotonation of the Schiff base. Determination of the precise conformation of the retinal and the position of water 402 and Asp85 at this time in the photocycle will undoubtedly advance our understanding of molecular events that lead to the deprotonation of the Schiff base.

Acknowledgements

I would like to thank Janos Lanyi for an exciting collaboration and for extensive discussions about my unconventional ideas. Robert Glaeser has been very supportive, in particular of my hydroxide pumping model. Jean-Philippe Cartailler did a lot of model building and refinement and was of great help in preparing numerous figures. Brigitte Schobert grows the best CLP crystals and kindly supplied figure 2A. Anja Rosengarth is our expert crystal aligner and she is also carrying out dynamic light scattering measurements on small unilamellar vesicles with oriented bacteriorhodopsin. Hans-Thomas Richter built the microspectrophotometer and recorded the crystal spectra in figure 2B. I would also like to thank the beamline staff at the Advanced Light Source (ALS, BL 5.0.2), at the European Synchrotron Radiation Facility (ESRF, ID13), and the Stanford Synchrotron Radiation Laboratory (SSRL, BL9-2) for their help. This work was supported by a grant from the NIH.

References

[1] J.K. Lanyi, J. Biol. Chem. 272 (1997) 31209–31212.
[2] J.K. Lanyi, J. Struct. Biol. 124 (1998) 164–178.
[3] D. Oesterhelt, Curr. Opin. Struct. Biol. 8 (1998) 489–500.
[4] U. Haupts, J. Tittor, D. Oesterhelt, Annu. Rev. Biophys. Biomol. Struct. 28 (1999) 367–399.
[5] J.K. Lanyi, in: G.A. Gerencher (Ed.), Electrogenic Cl^- Transporters in Biological Membranes, Springer Verlag, Berlin, 1994, p. 1–16.
[6] D. Oesterhelt, Isr. J. Chem. 35 (1995) 475–494.
[7] W.D. Hoff, K.H. Jung, J.L. Spudich, Annu. Rev. Biophys. Biomol. Struct. 26 (1997) 223–258.
[8] P. Mitchell, Nature 191 (1961) 144–148.
[9] J.K. Lanyi, G. Váró, Isr. J. Chem. 35 (1995) 365–386.
[10] A. Maeda, Isr. J. Chem. 35 (1995) 387–400.
[11] L. Zheng, J. Herzfeld, J. Bioenerg. Biomembr. 24 (1992) 139–146.
[12] T. Althaus, W. Eisfeld, R. Lohrmann, M. Stockburger, Isr. J. Chem. 35 (1995) 227–252.
[13] H. Luecke, H.T. Richter, J.K. Lanyi, Science 280 (1998) 1934–1937.
[14] H. Luecke, B. Schobert, H.T. Richter, J.-P. Cartailler, J.K. Lanyi, J. Mol. Biol. 291 (1999) 899–911.
[15] G.S. Harbison, J.E. Roberts, J. Herzfeld, R.G. Griffin, J. Am. Chem. Soc. 110 (1988) 7221–7223.
[16] R.R. Birge, T.M. Cooper, A.F. Lawrence, M.B. Masthay, C. Vasilakis, C.-F. Zhang, R. Zidovetzki, J. Am. Chem. Soc. 111 (1989) 4063–4074.
[17] R.R. Birge, T.M. Cooper, A.F. Lawrence, M.B. Masthay, C.-F. Zhang, R. Zidovetzki, J. Am. Chem. Soc. 113 (1991) 4327–4328.
[18] M.S. Braiman, R.A. Mathies, Proc. Natl. Acad. Sci. USA 79 (1982) 403–407.
[19] F. Siebert, W. Mantele, Eur. J. Biochem. 130 (1983) 565–573.
[20] K.J. Rothschild, P. Roepe, P.L. Ahl, T.N. Earnest, R.A. Bogomolni, S.K. Das Gupta, C.M. Mulliken, J. Herzfeld, Proc. Natl. Acad. Sci. USA 83 (1986) 347–351.
[21] A. Maeda, H. Kandori, Y. Yamazaki, S. Nishimura, M. Hatanaka, Y.S. Chon, J. Sasaki, R. Needleman, J.K. Lanyi, J. Biochem. (Tokyo) 121 (1997) 399–406.
[22] G. Váró, J.K. Lanyi, Biochemistry 30 (1991) 7165–7171.
[23] L. Zimányi, G. Váró, M. Chang, B. Ni, R. Needleman, J.K. Lanyi, Biochemistry 31 (1992) 8535–8543.
[24] K. Gerwert, B. Hess, J. Soppa, D. Oesterhelt, Proc. Natl. Acad. Sci. USA 86 (1989) 4943–4947.
[25] A.K. Dioumaev, H.T. Richter, L.S. Brown, M. Tanio, S. Tuzi, H. Saitô, Y. Kimura, R. Needleman, J.K. Lanyi, Biochemistry 37 (1998) 2496–2506.
[26] H.T. Richter, R. Needleman, H. Kandori, A. Maeda, J.K. Lanyi, Biochemistry 35 (1996) 15461–15466.
[27] H. Kandori, Y. Yamazaki, M. Hatanaka, R. Needleman, L.S. Brown, H.T. Richter, J.K. Lanyi, A. Maeda, Biochemistry 36 (1997) 5134–5141.
[28] R. Henderson, Annu. Rev. Biophys. Bioeng. 6 (1977) 87–109.
[29] R. Henderson, P.N. Unwin, Nature 257 (1975) 28–32.
[30] R. Henderson, J.M. Baldwin, T.A. Ceska, F. Zemlin, E. Beckmann, K.H. Downing, J. Mol. Biol. 213 (1990) 899–929.
[31] N. Grigorieff, T.A. Ceska, K.H. Downing, J.M. Baldwin, R. Henderson, J. Mol. Biol. 259 (1996) 393–421.
[32] A.E. Blaurock, W. Stoeckenius, Nature 233 (1971) 152–155.
[33] H.-J. Steinhoff, R. Mollaaghababa, C. Altenbach, K. Hideg, M. Krebs, H.G. Khorana, W.L. Hubbell, Science 266 (1994) 105–107.
[34] D.J. Müller, D. Fotiadis, A. Engel, FEBS Lett. 430 (1998) 105–111.

[35] H.M. Berman, J. Westbrook, Z. Feng, G. Gilliland, T.N. Bhat, H. Weissig, I.N. Shindyalov, P.E. Bourne, Nucleic Acids Res. 28 (2000) 235–242.
[36] S. Subramaniam, Curr. Opin. Struct. Biol. 9 (1999) 462–468.
[37] G.M. Sheldrick, T. Schneider, Methods Enzymol. 277 (1997) 319–343.
[38] E.M. Landau, J.P. Rosenbusch, Proc. Natl. Acad. Sci. USA 93 (1996) 14532–14535.
[39] G. Rummel, A. Hardmeyer, C. Widmer, M.L. Chiu, P. Nollert, K.P. Locher, I. Pedruzzi, E.M. Landau, J.P. Rosenbusch, J. Struct. Biol. 121 (1998) 82–91.
[40] E. Pebay-Peyroula, G. Rummel, J.P. Rosenbusch, E.M. Landau, Science 277 (1997) 1676–1681.
[41] L.O. Essen, R. Siegert, W.D. Lehmann, D. Oesterhelt, Proc. Natl. Acad. Sci. USA 95 (1998) 11673–11678.
[42] H. Michel, D. Oesterhelt, Proc. Natl. Acad. Sci. USA 77 (1980) 1283–1285.
[43] G.F.X. Schertler, H.D. Bartunik, H. Michel, D. Oesterhelt, J. Mol. Biol. 234 (1993) 156–164.
[44] H. Berlhali, P. Nollert, A. Royant, C. Menzel, J. Rosenbusch, E.M. Landau, E. Pebay-Peyroula, Structure 7 (1999) 909–917.
[45] M. Hatanaka, R. Kashima, H. Kandori, N. Friedman, M. Sheves, R. Needleman, J.K. Lanyi, A. Maeda, Biochemistry 36 (1997) 5493–5498.
[46] T. Marti, H. Otto, T. Mogi, S.J. Rösselet, M.P. Heyn, H.G. Khorana, J. Biol. Chem. 266 (1991) 6919–6927.
[47] K. Ihara, T. Amemiya, Y. Miyashita, Y. Mukohata, Biophys. J. 67 (1994) 1187–1191.
[48] O. Weidlich, B. Schalt, N. Friedman, M. Sheves, J.K. Lanyi, L.S. Brown, F. Siebert, Biochemistry 35 (1996) 10807–10814.
[49] S. Sonar, M.P. Krebs, H.G. Khorana, K.J. Rothschild, Biochemistry 32 (1993) 2263–2271.
[50] J.K. Delaney, U. Schweiger, S. Subramaniam, Proc. Natl. Acad. Sci. USA 92 (1995) 11120–11124.
[51] S.W. Lin, R.A. Mathies, Biophys. J. 56 (1989) 653–660.
[52] T.N. Earnest, P. Roepe, M.S. Braiman, J. Gillespie, K.J. Rothschild, Biochemistry 25 (1986) 7793–7798.
[53] A. Maeda, J. Sasaki, Y. Yamazaki, R. Needleman, J.K. Lanyi, Biochemistry 33 (1994) 1713–1717.
[54] M. Hatanaka, H. Kandori, A. Maeda, Biophys. J. 73 (1997) 1001–1006.
[55] H. Kandori, Y. Yamazaki, J. Sasaki, R. Needleman, J.K. Lanyi, A. Maeda, J. Am. Chem. Soc. 117 (1995) 2118–2119.
[56] H. Otto, T. Marti, M. Holz, T. Mogi, L.J. Stern, F. Engel, H.G. Khorana, M.P. Heyn, Proc. Natl. Acad. Sci. USA 87 (1990) 1018–1022.
[57] L.S. Brown, L. Bonet, R. Needleman, J.K. Lanyi, Biophys. J. 65 (1993) 124–130.
[58] L.J. Keefe, J. Sondek, D. Shortle, E.E. Lattman, Proc. Natl. Acad. Sci. USA 90 (1993) 3275.
[59] T.G. Ebrey, in: M. Jackson (Ed.), Thermodynamics of Membranes, Receptors and Channels, CRC Press, New York, 1993, pp. 353–387.
[60] J.K. Lanyi, Biochim. Biophys. Acta 1183 (1993) 241–261.
[61] Y. Cao, G. Váró, A.L. Klinger, D.M. Czajkowsky, M.S. Braiman, R. Needleman, J.K. Lanyi, Biochemistry 32 (1993) 1981–1990.
[62] M.K. Joshi, S. Dracheva, A.K. Mukhopadhyay, S. Bose, R.W. Hendler, Biochemistry 37 (1998) 14463–14470.
[63] M. Kates, S.C. Kushwaha, G.D. Sprott, Methods Enzymol. 88 (1982) 98–111.
[64] S. Subramaniam, M. Gerstein, D. Oesterhelt, R. Henderson, EMBO J. 12 (1993) 1–8.
[65] J. Vonck, Biochemistry 35 (1996) 5870–5878.
[66] D.L. Farrens, C. Altenbach, K. Yang, W.L. Hubbell, H.G. Khorana, Science 274 (1996) 768–770.
[67] A. Nicholls, K.A. Sharp, B. Honig, Proteins 11 (1991) 281–296.
[68] S.H. White, W.C. Wimley, Annu. Rev. Biophys. Biomol. Struct. 28 (1999) 319–365.
[69] S. Dracheva, S. Bose, R.W. Hendler, FEBS Lett. 382 (1996) 209–212.
[70] H. Luecke, B. Schobert, H.T. Richter, J.-P. Cartailler, J.K. Lanyi, Science 286 (1999) 255–260.
[71] S. Subramaniam, I. Lindahl, P. Bullough, A.R. Faruqi, J. Tittor, D. Oesterhelt, L. Brown, J.K. Lanyi, R. Henderson, J. Mol. Biol. 287 (1999) 145–161.
[72] M. Kataoka, H. Kamikubo, F. Tokunaga, L.S. Brown, Y. Yamazaki, A. Maeda, M. Sheves, R. Needleman, J.K. Lanyi, J. Mol. Biol. 243 (1994) 621–638.
[73] B. Borucki, H. Otto, M.P. Heyn, J. Phys. Chem. B 102 (1998) 3821–3829.
[74] S. Moltke, A.A. Nevzorov, N. Sakai, I. Wallat, C. Job, K. Nakanishi, M.P. Heyn, M.F. Brown, Biochemistry 37 (1998) 11821–11835.
[75] S. Subramaniam, D.A. Greenhalgh, P. Rath, K.J. Rothschild, H.G. Khorana, Proc. Natl. Acad. Sci. USA 88 (1991) 6873–6877.
[76] L.S. Brown, J.K. Lanyi, Proc. Natl. Acad. Sci. USA 93 (1996) 1731–1734.
[77] S.P. Balashov, E.S. Imasheva, R. Govindjee, T.G. Ebrey, Biophys. J. 70 (1996) 473–481.
[78] H.T. Richter, L.S. Brown, R. Needleman, J.K. Lanyi, Biochemistry 35 (1996) 4054–4062.
[79] M.S. Braiman, A.K. Dioumaev, J.R. Lewis, Biophys. J. 70 (1996) 939–947.
[80] H. Kamikubo, M. Kataoka, G. Váró, T. Oka, F. Tokunaga, R. Needleman, J.K. Lanyi, Proc. Natl. Acad. Sci. USA 93 (1996) 1386–1390.
[81] Y. Cao, G. Váró, M. Chang, B. Ni, R. Needleman, J.K. Lanyi, Biochemistry 30 (1991) 10972–10979.
[82] M. Holz, L.A. Drachev, T. Mogi, H. Otto, A.D. Kaulen, M.P. Heyn, V.P. Skulachev, H.G. Khorana, Proc. Natl. Acad. Sci. USA 86 (1989) 2167–2171.
[83] J. Tittor, C. Soell, D. Oesterhelt, H.-J. Butt, E. Bamberg, EMBO J. 8 (1989) 3477–3482.
[84] K. Edman, P. Nollert, A. Royant, H. Belrhali, E. Pebay-Peyroula, J. Hajdu, R. Neutze, E.M. Landau, Nature 401 (1999) 822–826.
[85] H. Luecke, B. Schobert, J.P. Cartailler, H.T. Richter, A. Rosengarth, R. Needleman, J.K. Lanyi (accepted).

[86] L.S. Brown, J. Sasaki, H. Kandori, A. Maeda, R. Needleman, J.K. Lanyi, J. Biol. Chem. 270 (1995) 27122–27126.
[87] A.T. Petkova, J.G.G. Hu, M. Bizounok, M. Simpson, R.G. Griffin, J. Herzfeld, Biochemistry 38 (1999) 1562–1572.
[88] P. Scherrer, M.K. Mathew, W. Sperling, W. Stoeckenius, Biochemistry 28 (1989) 829–834.
[89] S.O. Smith, H.J.M. De Groot, R. Gebhard, J. Courtin, J. Lugtenburg, J. Herzfeld, R.G. Griffin, Biochemistry 28 (1989) 8897–8904.
[90] J. Sasaki, L.S. Brown, Y.-S. Chon, H. Kandori, A. Maeda, R. Needleman, J.K. Lanyi, Science 269 (1995) 73–75.
[91] L.S. Brown, R. Needleman, J.K. Lanyi, Biochemistry 35 (1996) 16048–16054.
[92] P. Mitchell, Science 206 (1979) 1148–1159.
[93] S.P. Balashov, R. Govindjee, M. Kono, E. Imasheva, E. Lukashev, T.G. Ebrey, R.K. Crouch, D.R. Menick, Y. Feng, Biochemistry 32 (1993) 10331–10343.
[94] N. Guex, M.C. Peitsch, Swiss-PdbViewer v3.51, http://www.expasy.ch/spdbv/mainpage.html, 1997.
[95] T.A. Ceska, J. Struct. Biol. 127 (1999) 135–140.
[96] T.A. Ceska, J. Struct. Biol. 129 (2000) 100.